

Galaxy groups in the 2dF galaxy redshift survey: Large Scale Structure with Groups

Ariel Zandivarez^{1,2}, Manuel E. Merchán^{1,2} & Nelson D. Padilla³

¹ *Grupo de Investigaciones en Astronomía Teórica y Experimental, IATE, Observatorio Astronómico, Laprida 854, Córdoba, Argentina.*

² *Consejo de Investigaciones Científicas y Técnicas de la República Argentina.*

³ *Department of Physics, University of Durham, South Road, Durham, DH1 3LE, UK*

29 October 2018

ABSTRACT

We use the 2dF Galaxy Group Catalogue constructed by Merchán & Zandivarez to study the large scale structure of the Universe traced by galaxy groups. We concentrate on the computation of the power spectrum and the two point correlation function. The resulting group power spectrum shows a similar shape to the galaxy power spectrum obtained from the 2dF Galaxy Redshift Survey by Percival et al., but with a higher amplitude quantified by a relative bias in redshift space of $b_s(k) \sim 1.5$ on the range of scales analysed in this work, $0.025 < k/h\text{Mpc}^{-1} < 0.45$. The group two point correlation function for the total sample is well described by a power law with correlation length $s_0 = 8.9 \pm 0.3 h^{-1}\text{Mpc}$ and slope $\gamma = -1.6 \pm 0.1$ on scales $s < 20 h^{-1}\text{Mpc}$. In order to study the dependence of the clustering properties on group mass we split the catalogue in four subsamples defined by different ranges of group virial masses. Our results are consistent with a 40% increase of the correlation length s_0 when the minimum mass of the sample increases from $\mathcal{M}_{vir} > 5 \times 10^{12} h^{-1}M_\odot$ to $\mathcal{M}_{vir} > 1 \times 10^{14} h^{-1}M_\odot$. These computations allow a fair estimate of the relation described by the correlation length s_0 and the mean intergroup separation d_c for galaxy systems of low mass. Our results show that an empirical scaling law $s_0 = 4.7 d_c^{0.32}$ provides a very good fit to the results from this work, as well as to previous results obtained for groups and clusters of galaxies. The same law describes the predictions for dark matter haloes in N-body simulations of ΛCDM models. We also extend our study to the redshift space distortions of galaxy groups, where we find that the anisotropies in the clustering pattern of the 2dF group catalogue are consistent with gravitational instability, with a flattening of the redshift-space correlation function contours in the direction of the line of sight. The group pairwise velocities found from this analysis for a sample of groups with masses $\mathcal{M}_{vir} > 5 \times 10^{12} h^{-1}M_\odot$, are consistent with $\langle w^2 \rangle^{1/2} = (280_{-110}^{+50})\text{km/s}$, in agreement with ΛCDM cosmological simulations. The bias factor for the 2dF groups of moderate masses $\mathcal{M}_{vir} > 2 \times 10^{13} h^{-1}M_\odot$ is consistent with the values predicted by the combination of a CDM model and the ellipsoidal collapse model for the formation of structures.

Key words: galaxies: clusters: general - cosmology: large-scale structure of Universe.

1 INTRODUCTION

The position of groups of galaxies in the structure hierarchy makes them very interesting objects, as the density fluctuations sampled by groups lay between those traced by galaxies and clusters of galaxies. This is what makes the study of galaxy groups a key area of research in cosmology and galaxy formation. Much effort has been devoted to the study of groups in order to understand the large scale structure of the Universe (e.g., Jing & Zhang 1988, Maia & da Costa 1990, Ramella, Geller & Huchra 1990, Trasarti-Battistoni,

Invernizzi & Bonometto 1997). The main tool adopted in most of these works for the study of the spatial distribution of groups is the redshift space two point correlation function $\xi(s)$. These studies show, as expected from the hierarchical model, that the amplitude of the group $\xi(s)$ falls roughly between the corresponding amplitudes of correlations obtained from galaxies and cluster of galaxies. Using a suitable statistical sample of groups, Merchán, Maia & Lambas (2000) analysed the dependence of the two point correlation function on mass, by splitting the group sample in different ranges of virial mass, and extending this analysis to lower

mass systems (See also Bahcall & West, 1992, Croft et al. 1997, Abadi, Lambas & Muriel, 1998, Borgani et al. 1999, Collins et al. 2000). Their results show that the amplitude of $\xi(s)$ tends to increase significantly with the mass of the sample. They measure a 50% increase in correlation length for a sample with mean inter-group separation $d_c \simeq 28h^{-1}\text{Mpc}$ with respect to a sample with $d_c = 9h^{-1}\text{Mpc}$.

On the other hand, the measurement of the power spectrum of density fluctuations, a widely used statistical tool for galaxies and clusters of galaxies, has seldom been applied to the study of galaxy groups. This could be due to the fact that up to now, a statistically reliable sample of galaxy groups, from which a robust determination of the power spectrum can be made, has not been available.

Other important constraints on cosmological models can also be obtained from the study of the anisotropies in the redshift-space correlation function. The three-dimensional clustering information available in redshift surveys is subject to the influence of peculiar velocities on the distance measurements. This induces an anisotropy into the clustering pattern, which can be used to determine cosmological parameters due to the fact that the amplitude of peculiar velocities is related to the matter density, Ω , and the linear bias parameter, b . This study is carried out by measuring the apparent distortion of the clustering pattern in the two point correlation function in redshift space. On large scales, where the linear perturbation theory approximation for the growth of density fluctuation is valid, flows of mass from low to high density regions generate an artificial enhancement of the density contrast so as to produce a compression of the ξ contours along the line-of-sight direction (Kaiser 1987). This phenomenon allows estimates of the parameter $\beta \simeq \Omega^{0.6}/b$ to be made. On small scales, the main effect is to reduce the amplitude of density fluctuations by means of random non-linear motions in virialized regions, producing the ‘‘Fingers of God’’ effect. In this regime, it is possible to obtain estimates of the one-dimensional pairwise rms velocity dispersion (Davis & Peebles 1983). Such an analysis was recently applied to groups of galaxies identified in the Updated Zwicky Catalogue by Padilla et al. (2001). They found a one-dimensional pairwise rms velocity dispersion for groups of $250 \pm 110\text{km s}^{-1}$ and a noisy estimate of the β -parameter, $\beta < 1.5$. These results suggest the need for larger samples of groups in order to obtain more reliable results from these type of objects.

The 2dF Galaxy Group Catalogue (hereafter 2dFGGC), constructed by Merchán & Zandivarez (2002) is one of the largest group catalogues at present. These groups were identified from the 2dF public 100K data release using a modified Huchra & Geller (1982) group finding algorithm that takes into account the magnitude limit of the 2dF sample, redshift completeness, and angular masks (Colless et al. 2001). This sample of groups has been used to study the global effects of group environment on star formation (Martínez et al. 2002a), the effect of local environment on galaxy member spectral types (Domínguez et al. 2002), a statistical analysis of luminosity functions (Martínez et al. 2002b) and a compactness analysis of groups (Zandivarez et al. 2002).

In this work we use the 2dFGGC as a tracer of the large scale structure of the Universe and compute the power spectrum of galaxy group fluctuations and the two point correlation function. The sample is being splitted by taking

all galaxies above different cuts in virial mass in order to study the dependence of the clustering strength on group mass. Finally, we study the redshift-space distortions of the group two point correlation function and obtain estimates of the group pairwise velocities and the group bias factors.

The layout of this paper is as follows. In section 2 we describe the group catalogue, while in section 3 we present detailed information about the construction of the mock catalogues used in the clustering analysis. The methods for estimating the power spectrum and the two point correlation function using the 2dF group sample are described in section 4. Studies of the anisotropies present in the redshift-space correlation function are analysed in section 5. Finally, we summarise our conclusions in section 6.

2 THE 2DFGGC

Merchán & Zandivarez (2002) identified galaxy groups in the 2dF public 100K data release of galaxies within the southern (SGP, $-37^\circ.5 \leq \delta \leq -22^\circ.5$, $21^h40^m \leq \alpha \leq 3^h30^m$) and northern (NGP, $-7^\circ.5 \leq \delta \leq 2^\circ.5$; $9^h50^m \leq \alpha \leq 14^h50^m$) strips of the catalogue (see Colless et al. 2001). The group finder algorithm used in the identification is an adaptation of the algorithm developed by Huchra & Geller (1982), modified in order to take into account the incomplete sky coverage of the 100k release of 2dF galaxies.

The 2dFGGC was constructed using density contrast of $\delta\rho/\rho = 80$ and a fiducial linking length velocity of $V_0 = 200\text{km s}^{-1}$ which maximise the group finding accuracy (see section 4 of Merchán & Zandivarez 2002). The resulting group catalogue contains systems with at least 4 members, mean radial velocities in the range $900\text{km s}^{-1} \leq V \leq 75000\text{km s}^{-1}$ and a total number of 2198 groups (see Martínez et al. 2002b). The limit adopted in the number of members in galaxy groups is necessary in order to avoid pseudo-groups.

The virial group masses, \mathcal{M}_{vir} , are estimated using virial radii, R_V , and velocity dispersions, σ , $\mathcal{M}_{vir} = \sigma^2 R_V / G$. The R_V are computed using the projected virial radius and the σ using the virial radius along the line of sight (see section 5 in Merchán & Zandivarez 2002). A robust estimation of this component is obtained by applying the bi-weight estimator for groups with richness $N_{tot} \geq 15$ and the gapper estimator for poorer groups (Beers, Flynn and Gebhardt 1990, Girardi et al. 1993, Girardi and Giuricin 2000). These methods improve the velocity dispersion estimation in terms of efficiency and stability when dealing with small groups. The group catalogue has an average velocity dispersion of 265 km s^{-1} , an average virial mass of $9.1 \times 10^{13} h^{-1} M_\odot$ and an average virial radius of $1.15 h^{-1}\text{Mpc}$.

The analysis involving computation of comoving distances are carried out adopting the cosmological model parameters $\Omega_0 = 0.3$ and $\Omega_\Lambda = 0.7$.

3 MOCK CATALOGUES

Throughout this work we use a set of mock catalogues constructed from several cosmological numerical simulations of flat, low density, cold dark matter universes. We perform

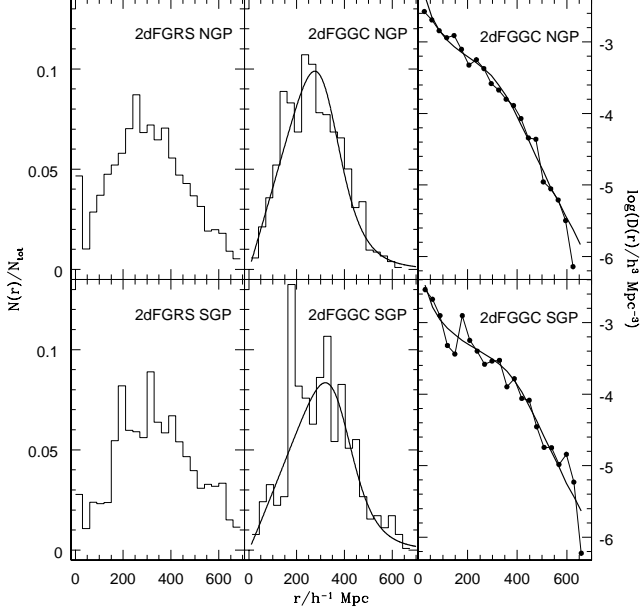


Figure 1. Distance distributions of 2dF 100k release galaxies and groups. The left panels show the normalised distance distributions of galaxies in the 2dF galaxy redshift survey (2dFGRS) splitted in the northern (NGP, upper panel) and southern (SGP, lower panel) strip. The centre panels show the normalised distance distributions for the group catalogue (2dFGGC), while the right panels show the radial density distributions for the same catalogue. The solid lines in centre and right panels show the best fitting functions obtained for the group distance distributions (see equation 6).

these simulations using the gravity part of the Hydra N-body code developed by Couchman et. al (1995), with 128^3 particles in a cubic comoving volume of $180 h^{-1}$ Mpc on a side starting at $z=50$. The adopted cosmological model corresponds to a universe with a present day matter density $\Omega_m = 0.3$, vacuum energy density $\Omega_\Lambda = 0.7$, baryon density $\Omega_b = 0.0$, spectral slope $n = 2$, $\Gamma = 0.21$, Hubble constant $H_0 = 100h \text{ km s}^{-1} \text{ Mpc}^{-1}$ with $h = 0.7$, and an amplitude of mass fluctuations of $\sigma_8 = 0.9$. In order to reproduce the same radial distribution as in the 2dFGRS, we adopt a galaxy luminosity function fitted by a Schechter function with $M_{b,J}^* - 5 \log_{10} h = -19.66$, $\alpha = -1.21$, $\Phi^* = 1.68 \times 10^{-2} h^3 \text{ Mpc}^{-3}$ and a model for the average k+e corrections given by the formula

$$k(z) + e(z) = \frac{z + 6z^2}{1 + 20z^3} \quad (1)$$

(Norberg et al. 2002). Consequently, we assign absolute magnitudes to the simulation particles in order to reproduce the previous luminosity function and compute the apparent magnitude for the particles lying within the 2dFGRS mask, using the equation

$$m = k + e + 5 \log_{10}(d_L/h^{-1} \text{ Mpc}) + 25 + (M_b - 5 \log_{10} h). \quad (2)$$

Then we apply the magnitude limited cuts using the magnitude limited mask of the 2dFGRS. In order to identify groups in the mock catalogues, we adopt the same values $\delta\rho/\rho = 80$ and $V_0 = 200 \text{ km s}^{-1}$ which maximise the group

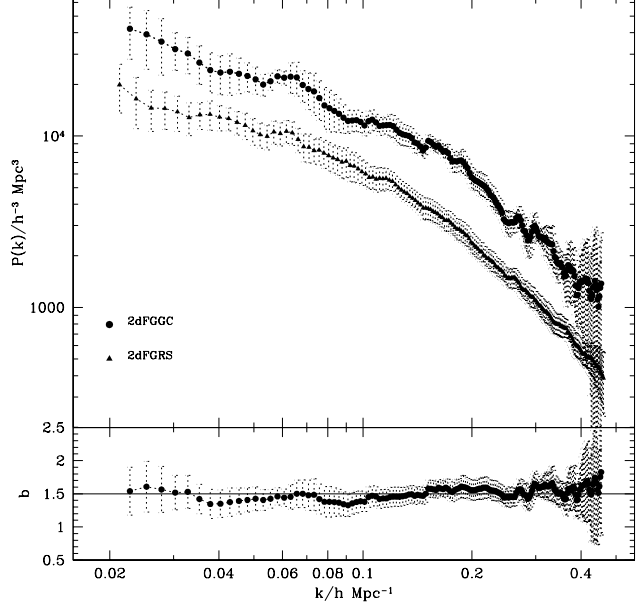


Figure 2. Upper panel: The comparison between the power spectrum of the groups in the 2dFGGC (circles) and the power spectrum of the galaxies in the 2dFGRS 100k release (triangles). The error bars are computed measuring the dispersion over 10 mock catalogues constructed from N-body simulations with a Λ CDM cosmology. Lower panel: The redshift space relative bias $b_s(k)$ between galaxies and groups in the 2dF survey. The error bars are computed using the usual formula of error propagation.

finding accuracy on the 2dFGGC. It should be stated that the resulting power spectra obtained with the mock group catalogues following the previous recipes are very good predictions of the observed one.

4 MEASURING THE SPATIAL DISTRIBUTION

4.1 The power spectrum

When calculating the power spectrum of the 2dFGGC we choose the method based on the Fast Fourier Transform (FFT) developed by Feldman, Kaiser & Peacock (1994, hereafter FKP) in the version described by Hoyle et al. (1999). We denote by N_g the number of groups in the catalogue, and use the vector positions \mathbf{x}_c to specify their positions. The following step in the FKP method is to construct an unclustered catalogue with the same geometry and radial selection function than the group sample. In order to minimise the contribution of Poisson errors to our uncertainties, this random catalogue should have a large number of points N_r , with vector positions \mathbf{x}_r . We define a quantity with mean value zero as:

$$\delta(\mathbf{k}) = \sum_{c=1}^{N_c} \omega(x_c) e^{i\mathbf{k}\cdot\mathbf{x}_c} - \alpha \sum_{r=1}^{N_r} \omega(x_r) e^{i\mathbf{k}\cdot\mathbf{x}_r} \quad (3)$$

where the first term on the right hand side is the Fourier transform of the spatial distribution of groups, and the second term is the Fourier transform of the window function

of the survey. Assuming Gaussian density fluctuations, FKP derive a weighting function

$$\omega(r) = \frac{1}{1 + \bar{n}(r)P_w(k)}, \quad (4)$$

that minimises the power spectrum variance, where $\bar{n}(r)$ is the mean radial density of the catalogue and $P_w(k)$ is the power spectrum. Given that in order to compute these weights we need an estimate of the power spectrum, we propose a constant value for $P_w(k)$ as an initial guess and then test the dependence of the results on this value. However, the result of a series of computations of the power spectrum varying this initial guess indicate that the assumed value of $P_w(k)$ is not critical. A more difficult issue is the assumed mean radial density for our catalogue. As has been stated in many works on the 2dFGRS, the 100k public release of the catalogue has a completeness mask that should be taken into account for a reliable $\bar{n}(r)$ estimation. In the computation of the power spectrum from the 2dF galaxies, Percival et al. (2001) dealt with this problem by adopting a mean radial density which depends on the position on the sky. In order to search for a possible variation of the radial distributions with the choice of 2dF strip of the catalogue, we show in Figure 1 the normalised distance distribution of the 2dFGGC in the northern (middle upper panel) and southern (middle lower panel) strips. The left panels show the same distribution for the galaxies in the 2dFGRS. The radial densities for the group catalogue are plotted in the right hand side panels also for both strips as in previous panels. From these histograms one can appreciate slight differences in the radial distribution of groups in different strips. Thus, in order to take into account this variation, we use different mean densities for the two strips in the group catalogue,

$$\bar{n} \longrightarrow \begin{cases} \bar{n}_1(r, \alpha, \delta) \longrightarrow NGP \\ \bar{n}_2(r, \alpha, \delta) \longrightarrow SGP \end{cases} \quad (5)$$

where the angular dependence (α, δ) is related to a correction that accounts for the redshift completeness mask of the 2dFGRS. This double prescription is also adopted for the construction of the random catalogues in order to impose more realistic radial selection functions. We use smooth curves which are the best fitting functions that describe the histograms showed in Figure 1. These functions are described by

$$N(r) = 2^{(1+x/y)} N_{max} \left(\frac{r}{r_{max}} \right)^x \left[1 + \left(\frac{r}{r_{max}} \right)^y \right]^{-(1+x/y)} \quad (6)$$

where the parameters are estimated using a chi-square maximum likelihood method. The fitting functions are plotted with solid lines in central and right panel of Figure 1. The best fitting parameters are $x = 1.02$, $y = 7.13$, $N_{max} = 71.44$ and $r_{max} = 362.34 h^{-1} \text{Mpc}$ for the NGP strip, and $x = 1.03$, $y = 7.98$, $N_{max} = 66.20$ and $r_{max} = 413.50 h^{-1} \text{Mpc}$ for the SGP strip.

In Equation 3 we use $\alpha = S_c/S_r$, where $S_c = \sum_{c=1}^{N_c} \omega^2(x_c)$ and $S_r = \sum_{r=1}^{N_r} \omega^2(x_r)$ in order to recover the definition of $P(\mathbf{k})$ given by equation (3.4.5) of FKP. Then, the power spectrum estimator is obtained by:

$$P(\mathbf{k}) = \frac{V(|\delta(\mathbf{k})|^2 - \alpha(1 + \alpha)S_r)}{\alpha^2 \sum_{i=1}^{N^3} (|W(\mathbf{k}_i)|^2 - S_r^{-1})}, \quad (7)$$

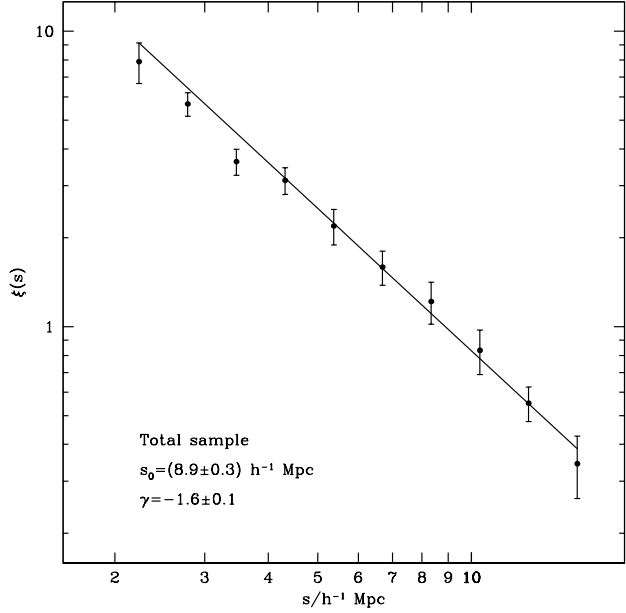


Figure 3. The two point correlation function for groups in the 2dFGGC. The error bars are estimated measuring the dispersion over 10 mock catalogues as previously applied in the power spectrum error computation. The solid line is the best power law approximation (eq 9, see legend).

where V is the volume over which periodicity is assumed. Finally, assuming isotropy we compute the power spectrum estimator averaging over spherical shells $k < |\mathbf{k}| < k + dk$ in k -space. We compute spectral densities at multiples of the fundamental mode in order to avoid oversampling of the spectrum that could result in spurious features. The computation of these quantities is carried out by embedding the distributions within a periodic cubic volume $V = r_{box}^3$ which is larger than the observational sample, and is divided into N cells per side with the spatial distribution of points (groups or random) assigned to the grid by means of the nearest grid point weight assignment scheme.

The fiducial values chosen for the parameters involved in the calculation of the power spectrum are the FFT grid dimension $N = 256$, the side of the box, $r_{box} = 2r_{min}$, where $r_{min} = 1244 h^{-1} \text{Mpc}$ is the side of the minimum box that contains the total catalogue (i.e., Nyquist frequency $\sim 0.32 h^{-3} \text{Mpc}^3$), a constant value of the power spectrum for the weight function of $P_w(k) = 20000 h^{-3} \text{Mpc}^3$, and a number of random points of $N_r = 1 \times 10^6$. The resulting power spectrum for the 2dFGGC is plotted with filled circles in the upper panel of Figure 2. The error bars of this estimate are computed using a set of 10 mock catalogues constructed as described in previous section. We also estimate the power spectrum for the galaxies in the 2dF survey with fiducial parameters $N = 512$ and $P_w(k) = 5000 h^{-3} \text{Mpc}^3$, obtaining very similar results to those obtained by Percival et al. (2001). Our estimate of the galaxy power spectrum is shown by filled triangles in the upper panel of Figure 2, where the error bars are also estimated from mock catalogues. As expected (Padilla & Baugh 2002), the power spectrum of galaxy groups has a very similar shape to the

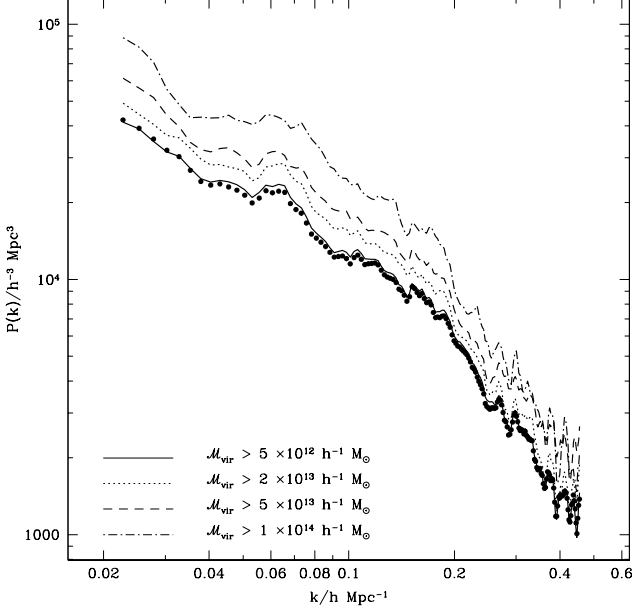


Figure 4. The power spectrum for different mass subsamples of the 2dFGGC. The solid line shows the power spectrum for groups with $\mathcal{M}_{vir} > 5 \times 10^{12} h^{-1} M_{\odot}$; dotted line shows the power spectrum for groups with $\mathcal{M}_{vir} > 2 \times 10^{13} h^{-1} M_{\odot}$; the dashed line displays the power spectrum for the subsample with $\mathcal{M}_{vir} > 5 \times 10^{13} h^{-1} M_{\odot}$, and the dashed-dotted line shows the corresponding power spectrum for the subsample in the range $\mathcal{M}_{vir} > 1 \times 10^{14} h^{-1} M_{\odot}$. The filled circles show the power spectrum for the whole sample.

result for galaxies but with a higher amplitude. This difference in amplitude can be measured computing the relative bias between the two power spectra defined by

$$b_s(k) = \sqrt{\frac{P_{grp}(k)}{P_{gal}(k)}}. \quad (8)$$

The bias function is plotted in the lower panel of Figure 2 where the error bars are computed from error propagation. It can be seen that the redshift-space bias parameter is almost constant $b_s(k) \sim 1.5$ for the full range of wave numbers, $0.025 < k/h\text{Mpc}^{-1} < 0.45$. It should be taken into account that this redshift-space bias function could differ from the real-space bias function. A possible relation between them will be discussed in section 5.

4.2 The two point correlation function

As a second method to measure the clustering properties of the galaxy groups in the 2dFGGC we estimate the redshift-space correlation function. This computation is carried out using the estimator proposed by Landy & Szalay (1993)

$$\xi(s) = \frac{DD - 2DR + RR}{RR}, \quad (9)$$

where DD , DR and RR are the suitably normalised number of data-data, data-random and random-random pairs respectively, in each separation bin. To estimate the two point correlation function, we generate a catalogue of randomly

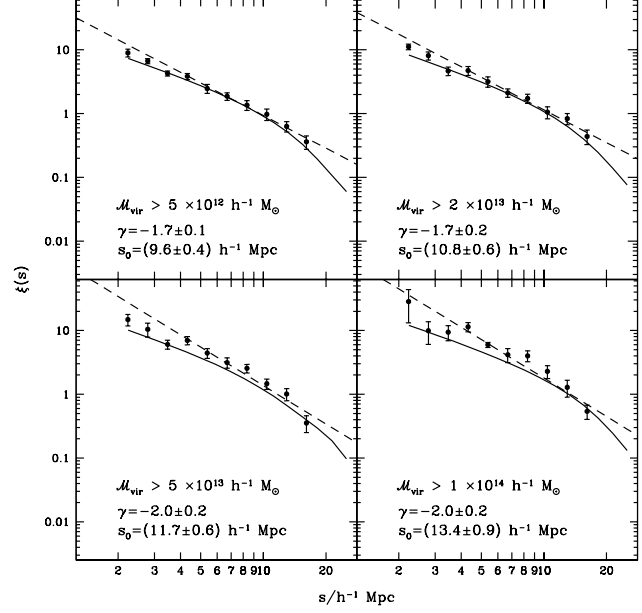


Figure 5. The two point correlation function for different mass subsamples of the 2dFGGC. The filled circles show the two point correlation function computed using the Landy & Szalay (1993) estimator (see equation 9). The dashed line corresponds to the best power law fit to the points (see labels), and the solid lines show the two point correlation function obtained from the integration of the corresponding power spectrum (see equation 11).

placed points with the same angular and radial selection function as the real data, as used for the computation of the power spectrum. We also take into account the completeness of the survey as a function of the position on the sky.

The resulting two point correlation function for groups in the 2dFGGC, plotted in Figure 3, shows a positive signal up to $20 h^{-1}\text{Mpc}$. We adopt a power law approximation for our estimate described by the formula

$$\xi(s) = \left(\frac{s}{s_0}\right)^\gamma \quad (10)$$

where s_0 is the correlation length and γ the logarithmic slope of the correlation function. From a Levenbergh-Marquardt method (Press et al. 1986) which takes into account errors and applies a minimum nonlinear least-squares, the best-fitting parameters obtained for our estimation are $s_0 = 8.9 \pm 0.3 h^{-1}\text{Mpc}$ and $\gamma = -1.6 \pm 0.1$. This result is consistent with previous estimates obtained from samples with comparable space densities, by Girardi, Boschin & da Costa (2000) ($s_0 = 8 \pm 1 h^{-1}\text{Mpc}$; $\gamma = -1.9 \pm 0.7$) and Merchán, Maia & Lambas (2000) ($s_0 = 9.0 \pm 0.4 h^{-1}\text{Mpc}$; $\gamma = -1.67 \pm 0.09$).

To test the dependence of the clustering of the 2dFGGC on the space density of our group samples, we study a set of subsamples defined by different ranges of virial masses which translate into values of mean inter-group separations, d_c . The adopted mass limits are

$$\text{Sample 1} \rightarrow \mathcal{M}_{vir} > 5 \times 10^{12} h^{-1} M_{\odot}$$

$$\text{Sample 2} \rightarrow \mathcal{M}_{vir} > 2 \times 10^{13} h^{-1} M_{\odot}$$

$$\text{Sample 3} \rightarrow \mathcal{M}_{vir} > 5 \times 10^{13} h^{-1} M_{\odot}$$

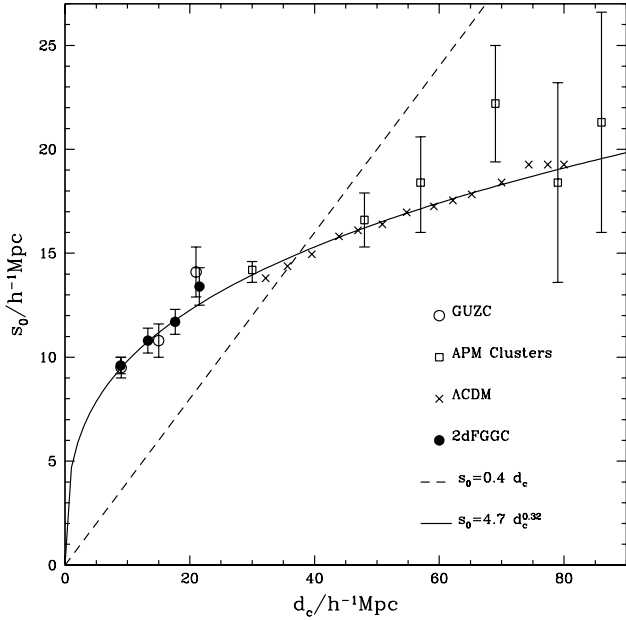


Figure 6. Correlation length s_0 as a function of the mean intergroup separation d_c . Filled circles correspond to the four subsamples defined in the 2dFGGC for different ranges of virial mass. Open circles show the determinations for subsamples of groups in the GUZC (Merchán, Maia & Lambas 2000). The open squares show the $s_0 - d_c$ relation of APM clusters, and crosses correspond to the prediction for a Λ CDM model, both determined by Croft et al. (1997). The dashed line represents the universal scaling law, $s_0 = 0.4 d_c$ (Bahcall & West 1992). The solid line is our fit to the data, $s_0 = 4.7 d_c^{0.32}$.

$$\text{Sample 4} \rightarrow \mathcal{M}_{\text{vir}} > 1 \times 10^{14} h^{-1} M_{\odot}$$

The analysis of these subsamples is carried out as follows. We compute the power spectrum for each subsample. These determinations can be considered to be statistically reliable due to the large number of groups in the 2dFGGC. Then, we make an estimate of $\xi(s)$ for each subsample using the relation between the power spectrum and the correlation function as Fourier transform pairs:

$$\xi(s) = \frac{1}{2\pi^2} \int_0^{\infty} P(k) k^2 \frac{\sin ks}{ks} dk. \quad (11)$$

And finally, we compare these determinations with those obtained from the computation of the two point correlation function for each subsample using Equation 9. In Figure 4 we display the power spectra obtained for each subsample. The filled circles in this figure correspond to the power spectrum for the full sample of groups. As expected, the amplitude of the power spectrum increases with the average mass of groups in the subsamples. If we are to estimate $\xi(s)$ using the determinations of $P(k)$ presented in this section, it should be taken into account that a reliable computation requires knowledge of the power spectrum over a wide range of k values. Since we only obtain $P(k)$ for $k \lesssim 0.4 h \text{ Mpc}^{-1}$, we extend our estimates to larger wavenumbers assuming a power law behaviour $P(k) \propto k^{-2}$. Consequently, we fit this power law to each subsample using values of $P(k)$ in the range $0.16 \lesssim k \lesssim 0.4 h \text{ Mpc}^{-1}$. The resulting power laws

obtained from a minimum nonlinear least-squares analysis are

$$\text{Sample 1} \rightarrow P(k) = 2.37 k^{-2} h^{-1} \text{Mpc}$$

$$\text{Sample 2} \rightarrow P(k) = 2.42 k^{-2} h^{-1} \text{Mpc}$$

$$\text{Sample 3} \rightarrow P(k) = 2.51 k^{-2} h^{-1} \text{Mpc}$$

$$\text{Sample 4} \rightarrow P(k) = 2.57 k^{-2} h^{-1} \text{Mpc}$$

With these extensions to large wavenumbers the two point correlation functions obtained applying Equation 11 to the results from each sample are plotted with solid lines in Figure 5. In this figure, the filled circles correspond to the direct estimate of $\xi(s)$ for each subsample using Equation 9. The error bars are computed using the set of 10 2dFGGC mock catalogues described in section 3. From this plot we observe that there is a good agreement between both methods of estimating $\xi(s)$. The dashed lines in each panel correspond to the best fit obtained for $\xi(s)$ assuming a power law shape (eq. 10). The best fitting parameters obtained for each subsample are shown in table 1.

Using the estimates of s_0 for each subsample, we proceed to study the $s_0 - d_c$ relation. The mean intergroup separations, d_c , are computed using the analytical mass function prediction based on the ellipsoidal collapse model of overdensities derived by Sheth & Tormen (1999) which is a very good fit to the 2dFGGC mass function measured by Martínez et al. (2002b). We compute the abundance $n(> \mathcal{M})$ of these systems in the ranges of masses defined for each subsample and estimate $d_c = n^{-1/3}$.

The resulting values of mean inter-group separation for the 2dFGGC subsamples are shown in table 1. The corresponding (d_c, s_0) pairs are shown in Figure 6 by filled circles. For comparison, we also plot previous determinations from groups in the Updated Zwicky Catalogue (GUZC) derived by Merchán, Maia & Lambas (2000) which shown a very similar behaviour with our results. The $s_0 - d_c$ pairs shown in the range of scales corresponding to clusters of galaxies are those obtained from the APM cluster survey by Croft et al. (1997, open squares). In previous works, some authors (Bahcall & West 1992, Bahcall & Cen 1992) have argued that Abell clusters are consistent with a linear $s_0 - d_c$ relation described by $s_0 = 0.4 d_c$. This scaling law is plotted as a dashed line in Figure 6 and does not seem to provide a good description either of cluster data or of groups of galaxies. This result was also reached by Croft et al. (1997) where they also computed the $s_0 - d_c$ relation for clusters of galaxies in a Λ CDM N-body simulation. Their results are represented by crosses in Figure 6. As can be seen, our estimate of the $s_0 - d_c$ relation for groups is an extension of the relation obtained by Croft et al. (1997) from numerical simulations from a Λ CDM model. Similar trends in $s_0 - d_c$ were also found in other CDM models, but with slightly different amplitudes of correlation length (see Governato et al. 1999). We find that a simple fit of the form

$$s_0 = 4.7 d_c^{0.32} \quad (12)$$

provides a satisfactory empirical description of the observational data as well as the N-body simulation results. This empirical scaling law is shown by the solid line in Figure 6.

5 REDSHIFT SPACE DISTORTIONS

In this section we study the redshift-space correlation function calculated in the directions parallel and perpendicular to the line of sight, $\xi(\sigma, \pi)$. This approach has led to the quantification of characteristics of the redshift-space distribution of galaxies and clusters of galaxies, such as the “fingers of God”, which are elongated structures seen in redshift surveys, originating from the random motions of galaxies inside clusters. The statistics that can be derived from the anisotropies in $\xi(\sigma, \pi)$ are presented in section 5.1 and the results found for the different 2dFGGC subsamples can be found in section 5.2. Section 5.3 contains the results for pairwise velocities corresponding to the different subsamples, and 5.4 the corresponding bias factors.

5.1 Statistics from the anisotropies in the redshift-space correlation function

The quantification of the “fingers of God” effect comes from the measurement of the pairwise velocities of galaxies, which can be done by comparing a theoretical expression for the correlation function, $\xi^p(\sigma, \pi)$, with the measured values, $\xi^o(\sigma, \pi)$ (the index o indicates quantities measured from observational data, and the index p denotes predicted quantities). Specifically, we compare curves of equal correlation function amplitude (ξ^{fix}) parametrised by $r_{\xi^{fix}}^o(\theta)$ and $r_{\xi^{fix}}^p(\theta)$, where θ is the angle measured from the direction perpendicular to the line of sight (Padilla et al. 2001), such that $\xi^o(\sigma_r, \pi_r) - \xi^{fix} = 0$, where $\sigma_r = r_{\xi^{fix}}^x(\theta) \cos(\theta)$, $\pi_r = r_{\xi^{fix}}^x(\theta) \sin(\theta)$, and the index x indicates either observed (o) or predicted quantities (p).

The predicted correlation function is obtained by convolving the real-space correlation function, $\xi(r)$ with the pairwise velocity distribution function, $f(w)$, following Bean et al. (1983). In order to do this, we calculate

$$1 + \xi^p(\sigma, \pi) = \int_{-\infty}^{\infty} [1 + \xi(r)] f[w' - w^s(r, r')] dw', \quad (13)$$

where $r^2 = r'^2 + \sigma^2$, and H_0 is the Hubble constant, $r' = \pi - w'/H_0$ (the prime denotes the line-of-sight component of a vector quantity) and

$$w^s(r, r') \simeq -H_0 \beta \xi(r) (1 + \xi(r))^{-1} r', \quad (14)$$

is the mean streaming velocity of galaxies at separation r .

Following the usual prescription, we calculate the best-fit rms peculiar velocity, $\langle w^2 \rangle^{1/2}$, for an exponential distribution,

$$f(w) = \frac{1}{\sqrt{2} \langle w^2 \rangle^{1/2}} \exp\left(-\sqrt{2} \frac{|w|}{\langle w^2 \rangle^{1/2}}\right). \quad (15)$$

We adopted this pairwise velocity distribution as it has shown to be the most accurate fit to the results from numerical simulations (Ratcliffe et al. 1998, Padilla & Baugh 2002).

In this work we use a non-linear CDM correlation function, for which we assume a given cosmology. In order to do this, we follow the recent results from satellite and balloon borne cosmic microwave background experiments such as WMAP (Spergel et al. 2003) and Boomerang (Netterfield et al. 2002), and assume a Λ CDM cosmology with mass density $\Omega_0 = 0.28$, baryon density $\Omega_b = 0.05$, vacuum energy

density $\Omega_\Lambda = 0.67$, and a CDM shape parameter $\Gamma = 0.18$, and $\sigma_8 = 0.9$. These parameters are compatible with constraints from CMB data. Even though we include explicitly a baryon fraction in our models, the high level of noise of our observational data allow us only to measure the damping in power produced by baryons. This means that our choice of Γ implicitly allows for a combination of baryon fraction and a real value of Γ as discussed in Eisenstein & Hu (1996). We obtain the real-space correlation function by Fourier transforming the CDM power spectrum

$$\xi^{CDM}(r) = \frac{1}{2\pi^2} b^2 \int_0^\infty P(k) \frac{\sin(kr)}{kr} k^2 dk, \quad (16)$$

and then use this to evaluate the theoretical prediction for $\xi^p(\sigma, \pi)$ using equation (13). Here we assume a constant, scale independent, bias between the distribution of groups and mass, which has been shown to be a good approximation for groups and clusters of galaxies (Padilla & Baugh, 2001). Furthermore, by looking at figure 3, it can be seen that the values of correlation function slopes, γ , for the different samples are not significantly different (less than 1.3σ away); also, figure 2 shows that a constant relative bias is a good approximation up to scales $k < 0.45h/\text{Mpc}$, equivalent to $x \sim 10h^{-1}\text{Mpc}$, where our analyses take place.

We search for the optimum values of the scale independent bias parameter b and $\langle w^2 \rangle^{1/2}$ by minimising the quantity $\chi^2(\langle w^2 \rangle^{1/2}, b)$,

$$\chi^2(\langle w^2 \rangle^{1/2}, b) = \sum_i [r_{\xi^{fix}}^o(\theta_i) - r_{\xi^{fix}}^p(\theta_i)]^2, \quad (17)$$

where we have chosen to compare a set of discrete levels, $\xi^{fix} = 0.6, 0.8, 1.0, 1.2$ and 1.4 , of the redshift-space correlation function $\xi(\sigma, \pi)$ amplitude (Padilla et al. 2001) instead of comparing values of the correlation function on a grid of σ and π distances as done previously in other works (see for instance Ratcliffe et al. 1998).

5.2 Measurements of 2dfGGC $\xi(\sigma, \pi)$

Using the estimator represented by equation (9), we measure the redshift-space correlation function of the 2dFGGC for the four subsamples studied in this paper. In this case, the quantities DD , RR , and DR depend upon the separations parallel and perpendicular to the line of sight. The results can be seen in Figure 7 where the different panels show the correlation function for subsamples 1,2,3 and 4 (left to right hand side panels respectively).

Concentrating on the anisotropies we observe in this figure, we find that the infall pattern expected from gravitational instability is seen in most of the group subsamples with the exception of subsample 3. Here we should bear in mind the increasingly noisy results that are obtained for the samples of higher virial masses. This is a simple consequence of the ever smaller number of more massive objects that adds a Poisson error of increasing magnitude to the estimate of the correlation function. Still, subsamples 1, 2 and 4 show the infall pattern for many contour levels.

By inspecting the correlation lengths depicted by the thick solid lines in the panels of Figure 7, the increase in correlation length for subsamples with higher low virial mass limits is noticeable. This is in agreement with the direct mea-

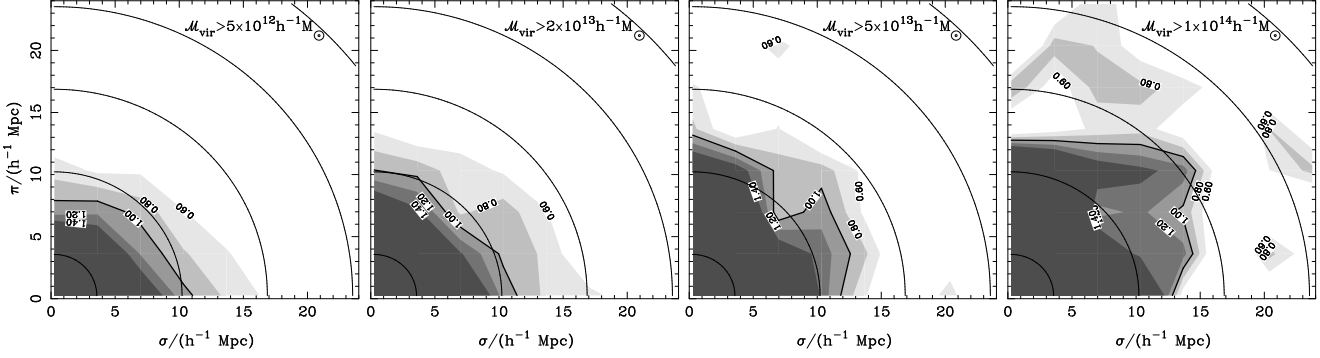


Figure 7. The 2-point correlation function of the four subsamples of 2dFG groups studied in this paper, in the coordinates σ and π (subsamples 1 to 4 from left to right hand side panels). The transitions between different shadings correspond to fixed values of $\xi = 0.6, 0.8, 1.0, 1.2$, and 1.4 levels, which are the values used later to infer the pairwise velocities, $\langle w^2 \rangle^{1/2}$. The thick line corresponds to the $\xi = 1$ level, and the thin lines show the expected contours in the absence of peculiar velocities.

Table 1. Statistical results for the 2dFGGC. The first columns show several characteristics of the different 2dFGGC samples, including the minimum virial mass of the groups in each sample, number of groups, their average distance, the average number of galaxy members identified per group, and the average internal velocity dispersion as measured from the identified member galaxies. Columns 7 and 8 show the correlation function fit parameters, column 9 contains the values of mean inter-group separation, and the last two columns, the corrected values of group pairwise velocity and bias factors obtained from the redshift-space distortions analysis.

Sample	\mathcal{M}_{vir} min. [$h^{-1}M_{\odot}$]	N_{grp}	$\langle zc \rangle$ [km s^{-1}]	n_{member}	σ_v [km s^{-1}]	s_0 [$h^{-1}\text{Mpc}$]	γ	d_c [$h^{-1}\text{Mpc}$]	$\langle w^2 \rangle_c^{1/2}$ [km s^{-1}]	b_r^{ξ}
All		2198	---	---	265 ± 150	8.9 ± 0.3	-1.6 ± 0.1	---	---	1.82 ± 0.36
Sample 1	5×10^{12}	1996	30333	6.9 ± 4.6	283 ± 149	9.6 ± 0.4	-1.7 ± 0.1	8.94	280^{+50}_{-110}	1.92 ± 0.38
Sample 2	2×10^{13}	1448	33035	7.5 ± 5.0	333 ± 143	10.8 ± 0.6	-1.7 ± 0.2	15.00	395^{+35}_{-95}	2.04 ± 0.41
Sample 3	5×10^{13}	920	36336	8.2 ± 5.8	396 ± 141	11.7 ± 0.6	-2.0 ± 0.2	20.93	540^{+40}_{-100}	2.24 ± 0.45
Sample 4	1×10^{14}	540	38631	8.6 ± 6.4	464 ± 142	13.4 ± 0.9	-2.0 ± 0.2	28.93	495^{+35}_{-175}	2.51 ± 0.50

measurements of redshift-space correlation function performed in section 4.2.

5.3 Pairwise velocities and correlation lengths in observational cluster samples

In order to summarise the results obtained from the study of the anisotropies in the correlation function of 2dFGGC subsamples, we present the values of pairwise velocities obtained from the correlation functions shown in Figure 7.

We find the group pairwise velocities by minimising equation 17. The real space correlation function used in this equation corresponds to a CDM power spectrum with spectral index $n_s = 1.0$, and parameters $\Omega_0 = 0.28$, $\Omega_{\Lambda} = 0.67$, a baryon density $\Omega_b = 0.05$, a CDM shape parameter $\Gamma = 0.18$, and $\sigma_8 = 0.9$.

The results for the pairwise pairwise velocities found from the correlation functions of the four 2dFGGC subsamples studied here are presented in Figure 8. The errorbars correspond to a $1 - \sigma$ standard deviation, calculated using 5 estimates of pairwise velocities obtained from 5 different correlation function level contours. We note that this is at best a lower limit to the uncertainty in $\langle w^2 \rangle^{1/2}$, since the results from different $\xi(\sigma, \pi)$ can be highly correlated. The ordering of samples is such that an increase in the x direc-

tion corresponds to an increase in the sample's lower virial mass limit.

The assumption that structures form by hierarchical clustering implies that the values of pairwise velocities found for these subsamples should have been smaller for higher mass limits, since more massive objects take longer to form virialized structures. This trend is expected in the direct measurements of pairwise velocities of groups identified from a Λ CDM simulation. In order to test this hypothesis we take 20 subsets of groups with the same mass limits and number of members as the 2dFGGC subsamples from the simulation, and measure their 1-dimensional pairwise velocities. The downward hatched region in Figure 8 corresponds to the 1- σ confidence levels for the group pairwise velocities from the numerical simulations. Even though the trend of decreasing pairwise velocities for higher masses is visible in the simulation results, the errors make it also consistent with a constant value. As can be seen, the agreement between subsample 1 and the simulations is remarkable. However, more massive groups in subsamples 2, 3 and 4 show higher values of $\langle w^2 \rangle^{1/2}$. This behaviour is in the opposite direction to what we expected from hierarchical clustering arguments. A possible cause for this disagreement is the likely inclusion of spurious groups affecting the low mass sample. However, as shown by Padilla & Lambas (2003a), this would produce an enhancement of the pairwise velocities, and therefore our

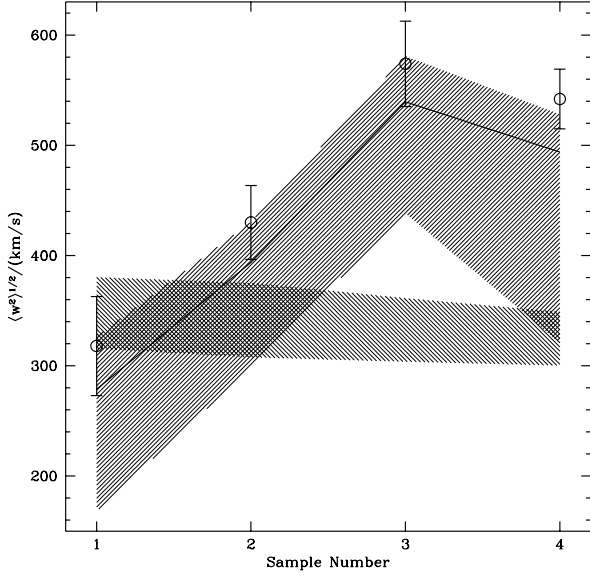


Figure 8. Pairwise velocities obtained for the different 2dFGGC subsamples (open symbols with errorbars). The samples are distributed along the x-axis, with samples of increasing lower virial mass limit towards the right. Errorbars are obtained from the estimates of pairwise velocities at 5 different correlation function contour levels. The solid line shows the corrected pairwise velocities obtained by subtracting in quadrature the error in the distance measurement of groups, and the corresponding $1-\sigma$ confidence level is represented by the upward hatched region. The downward hatched region shows the $1-\sigma$ confidence level obtained from 20 subsamples of groups identified from a Λ CDM simulation. Each of these subsamples contain the same number of groups as the 2dFGGC subsamples.

results for sample 1 would be overestimated, making the disagreement more severe. However, Padilla & Lambas (2003a) also show that in the case of groups identified from redshift surveys, this effect is not important. Another possible factor influencing our results is the increasing values of the average distance to groups in more massive subsamples, which is brought by selection function effects. The average group distance in subsamples 1,2,3, and 4, is larger for the most massive samples, as can be seen in Table 1. It is possible that the increase in average distance translates into a larger distance measurement error, which in turn tends to enhance the anisotropies in the correlation function along the line of sight, thus explaining the results obtained here. It should be noted though, that the amplitude of errors needed to obtain agreement with the simulations is small. For instance, for samples 3 and 4, a distance measurement error of $\Delta\langle w^2 \rangle^{1/2} \simeq 450 \text{ km/s}$ is enough to explain the discrepancies between the results from observations and the numerical simulation. This error is equivalent to a 1% uncertainty in the group distance measurements at the mean depth of these subsamples (see Table 1).

The origin of the uncertainty in the group distance measurement can be related to the fact that the number of galaxies (n_{member}) used in the distance determination of the groups shows little change among the subsamples, whereas the internal velocity dispersion of galaxies in groups (σ_v) shows a clear enhancement (see average values of n_{member}

and σ_v in Table 1). An expression for this uncertainty as a consequence of the finite number of galaxy distance measurements per group is,

$$\Delta(cz) = \frac{\sigma_v}{\sqrt{n_{member}}}, \quad (18)$$

which is based on the assumption that these galaxies were randomly selected from a gaussian distribution in redshift-space, of width σ_v . Using the average n_{member} in the group subsamples, we subtract $\sqrt{(2)\Delta(cz)}$ in quadrature from the estimate of $\langle w^2 \rangle^{1/2}$, and show the corrected $\langle w^2 \rangle_c^{1/2}$ in a solid line in Figure 8 as a function of subsample number. The upward hatched region shows the range covered by a $1-\sigma$ uncertainty in $\langle w^2 \rangle_c^{1/2}$, as it results from considering the widths of the distributions in n_{member} and σ_v for the individual group subsamples, and the original uncertainty in $\langle w^2 \rangle^{1/2}$ (the widths in n_{member} and σ_v are given in Table 1 as the uncertainty in these quantities). As can be seen, the corrected values are only slightly smaller than the original $\langle w^2 \rangle^{1/2}$. However, the amplitude of the uncertainties is noticeably increased, improving in most of the cases the agreement with the Λ CDM simulation. This is not enough to obtain an agreement for subsample 3, though, which had also failed in showing the expected infall pattern in figure 7.

We remark however that the assumed value of σ_8 also influences our results on $\langle w^2 \rangle^{1/2}$, but to a lesser extent. Assuming $\sigma_8 = 0.7$ lowers our estimates of pairwise velocity by $\simeq 10\%$, but leaves the uncertainty unchanged. However, we bear in mind the fact that these uncertainties can be underestimated due to correlations between the individual estimates of $\langle w^2 \rangle^{1/2}$, as explained above.

Another important point to be noticed is that even for sample 3 (our sample with no infall pattern), the obtained value of corrected group pairwise velocity $\langle w^2 \rangle_c^{1/2}$ remains one of the lowest values found for systems of galaxies (see Padilla & Lambas 2003b for a comprehensive analysis of several cluster samples), and is still in agreement with the pairwise velocities found for galaxy catalogues $\langle w^2 \rangle^{1/2} \simeq (450 \pm 100) \text{ km/s}$ (Ratcliffe et al. 1998, Padilla et al. 2001).

5.4 Bias factors

The comparison between the measured and predicted redshift-space correlation functions, as explained in section 2, involves the real-space bias (b_r^ξ) between the group and mass distributions, where the latter is described by a CDM model. In this work, we measure b_r^ξ by minimising $\chi^2(\langle w^2 \rangle^{1/2}, b_r^\xi)$ (eq. 17), where $\langle w^2 \rangle^{1/2}$ corresponds to the group pairwise velocities found in the previous section. As mentioned above, χ^2 depends upon the real space correlation function which is obtained from a CDM power spectrum with a fixed set of cosmological parameters (see previous section). We minimise χ^2 , and show the resulting bias factors in Figure 9 (open circles with errorbars) where the x-axis shows the 2dFGGC subsamples in order of increasing group mass. The errors on the bias parameter come from the results of minimising equation (17) for 5 different levels of the correlation function. We also include a 20% error added in quadrature to allow for an uncertainty in the assumed value of $\sigma_8 = 0.9$ (for instance, assuming $\sigma_8 = 0.7$ would produce an enhancement of a 13% in our estimates of bias factors). The values of bias factors and their uncertainties can be

found in Table 1, where we also show the result obtained for the full 2dFGGC sample.

These values can be compared to what is expected from a particular CDM model, using the expression for an effective CDM bias as presented in Padilla & Baugh (2002), which is a weighted average of the bias of a sample of clusters of mass M , derived by Sheth, Mo & Tormen (2001), and requires knowledge of the space density of the cluster sample. The results from using this equation are valid if the cluster sample is complete above a minimum mass threshold. The main source of systematics arising from this assumption comes from a possible underestimation of the space density induced by the incompleteness of the group sample. However, a lower limit for the completeness of the 2dFGGC subsamples is $\simeq 0.7$, and would only induce a change of $\simeq 5\%$ in the CDM bias factor.

The hatched region in figure 9 shows the range of expected values of a CDM bias factor for the same space densities present in the 2dFGGC subsamples, assuming $0.75 < \sigma_8 < 0.9$ (a larger σ_8 corresponds to a lower CDM bias factor). As can be seen, the 2dFGGC groups bias factor tends to increase with the minimum virial mass of the sample as expected from hierarchical clustering. Furthermore, the CDM bias is within the $1 - \sigma$ confidence levels around the measured bias factors for most of the samples, the exemption being the least massive subsample, for which the expected CDM bias factor is smaller. We investigated the effects of an underestimation of the group pairwise velocities on the value of the bias, and found that an increase of a factor ~ 2 in $\langle w^2 \rangle^{1/2}$ is enough for obtaining a result compatible with the CDM expectations.

As mentioned above, there is a possible $\simeq 5\%$ systematic error in the CDM bias factors. In order to visualise the effects of such an error, we show two solid lines in figure 9 which limit the range of CDM bias factors after correcting for this systematic error. As can be seen, this does not significantly affect the comparison between the 2dFGGC and CDM model biases.

The bias factors calculated in this section correspond to real space quantities and are relative to the distribution of mass which has an assumed amplitude of density fluctuations $\sigma_8 = 0.9$. On the other hand, the relative bias found from the ratio between the galaxy and group power spectra in section 4.1, $b_s(k)$, corresponds to a redshift space quantity, and is relative to the distribution of galaxies. The fact that this value corresponds to redshift-space, allows us to make a rough estimate of what would the corresponding real-space value be, based on the studies of Padilla & Baugh (2002), who find that the ratio between real and redshift space biases for cluster samples is roughly $b_r/b_s = 1.25$. Assuming that this relation can be also applied to the 2dFGGC, the redshift-space bias factor found from the power spectrum analysis corresponds to a real-space $b_r(k) = 1.9 \pm 0.4$, in the range of scales studied in this paper, $0.025 < k/h\text{Mpc}^{-1} < 0.45$, consistent with our estimates of the real-space bias parameter from the anisotropies in the correlation function. Assuming a different value of $\sigma_8 = 0.7$ produces no significant changes in this result.

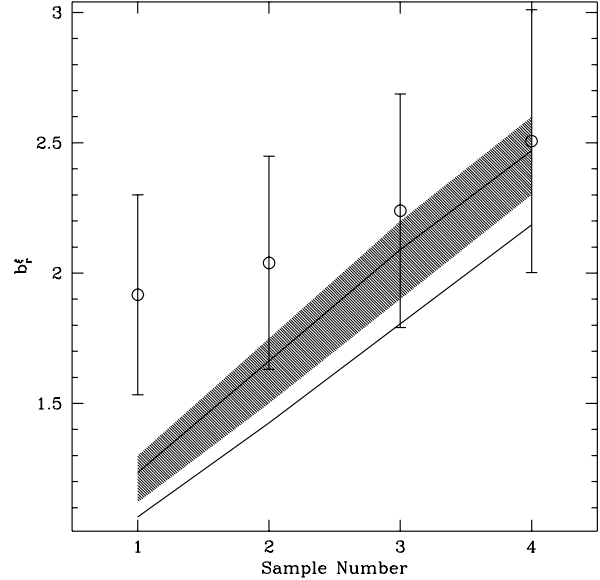


Figure 9. Bias factors for the 2dFGGC subsamples studied in this paper. The circles with errorbars show the results from minimising equation 17, and the hatched region shows the range of predicted effective bias from CDM and the Sheth, Mo & Tormen (2001) mass function for $0.75 < \sigma_8 < 0.9$. The solid lines limit the same range, after correcting for a systematic error $\simeq 5\%$. The different samples are displayed along the x-axis, ordered in such a way as to have higher virial masses towards the right.

6 CONCLUSIONS

We analysed the 2dFGGC constructed by Merchán & Zandivarez (2002), one of the largest group catalogues constructed at present. Our analysis considers galaxy groups as tracers of the large scale structure in the universe. The statistical tools adopted for this work are the power spectrum of density fluctuations and the two point correlation function, both calculated using redshift-space data. We calculated the group power spectrum and found that its shape is very similar to that of the galaxy power spectrum, but shows a higher amplitude as expected for higher mass systems in hierarchical clustering. The measurement of a relative bias between groups and galaxies in redshift space quantifies this difference in amplitude, and results in an almost constant relative bias value of $b_s(k) \sim 1.5$ on the scales probed by our analysis, $0.025 < k/h\text{Mpc}^{-1} < 0.45$.

The estimate of the two point correlation function for the group sample is found to be well fitted by a power law of the form $\xi = (s/s_0)^\gamma$ with a correlation length $s_0 = 8.9 \pm 0.3 h^{-1}\text{Mpc}$ and a slope $\gamma = -1.6 \pm 0.1$.

We also analyse the variation of the 2dFGGC groups clustering with group mass by studying the $s_0 - d_c$ relation. For this purpose, we split the group sample in four subsamples according to different ranges of group virial masses. Firstly, we check that the computation of the correlation function for each subsample using the direct method defined by Landy & Szalay (1993), yields a remarkably similar result to that obtained by Fourier transforming the corresponding power spectrum estimate. Secondly, the obtained correlation length s_0 tends to increase when using more massive samples

as previously observed by Merchán, Maia & Lambas (2000, see Table 1).

From the computation of the mean intergroup distance d_c , the resulting $s_0 - d_c$ relation is quite similar to that obtained by Merchán, Maia & Lambas (1993) for the GUZC. If we extend this relation with the $s_0 - d_c$ relation obtained for cluster of galaxies by Croft et al. (1997) we observe that the universal scaling law of Bahcall & West (1992), $s_0 = 0.4 d_c$, provides a poor description to the data. We find that a fit described by the law $s_0 = 4.7 d_c^{0.32}$, is capable of describing both, the observational $s_0 - d_c$ relation found for groups and clusters, as well as the results from N-body numerical simulations of a Λ CDM model presented by Croft et al. (1997, see also Governato et al. 1999).

The results from the study of the anisotropies in the redshift space correlation function show that in general, the groups in the 2dFGGC present the expected infall pattern indicating that these systems have not yet formed virialized structures themselves. This can be seen from the correlation function contours of sample 1, which includes the majority of the 2dFGGC groups.

The study of the redshift-space correlation functions also allowed us to make an estimate of the groups bias factor relative to the distribution of the mass. In order to achieve this, it was necessary to assume a CDM model with a fixed value of $\sigma_8 = 0.9$. We compare our estimates of bias factors to what is expected for such a cosmological model, where the mass function is well described by the Sheth, Mo & Tormen (2001) model. We find very good agreement for the samples 2, 3 and 4.

We calculate the group pairwise velocities for the different 2dFGGC subsamples, and correct them from group distance uncertainty effects ($\langle w^2 \rangle_c^{1/2}$, see table 1). We note that the pairwise velocity measured for samples 1 and 2, $\langle w^2 \rangle_c^{1/2} = (280_{-110}^{+50})$ km/s and $\langle w^2 \rangle_c^{1/2} = (395_{-95}^{+35})$ km/s, are noticeably smaller than that found for galaxies, $\langle w^2 \rangle^{1/2} = (450 \pm 100)$ km/s, in agreement with gravitational instability expectations. This agreement comes not only from a group pairwise velocity which is qualitatively smaller than the measurements found for galaxies, but also from a comparison with measurements from actual simulated groups, embedded in one of the most readily motivated cosmological scenarios, a Λ CDM model.

ACKNOWLEDGMENTS

We thank Mario Abadi, Vincent Eke, and Carlton Baugh for helpful comments and suggestions. We thank the Referee for invaluable comments and advice which helped improve the previous version of this paper. We also thank Peder Norberg and Shaun Cole for kindly providing the software describing the mask of the 2dFGRS and to the 2dFGRS Team for having made available the actual data sets of the sample. This work has been partially supported by Consejo de Investigaciones Científicas y Técnicas de la República Argentina (CONICET), the Secretaría de Ciencia y Técnica de la Universidad Nacional de Córdoba (SeCyT), Fundación Antorchas, Argentina, and the PPARC Rolling Grant at Durham.

REFERENCES

- Abadi M.G., Lambas D.G., Muriel H., 1998, ApJ, 507, 526.
 Bahcall N.A., Cen R., 1992, ApJ, 398, L81.
 Bahcall N.A., West M., 1992, ApJ, 392, 419.
 Bean, A.J., Efstathiou, G., Ellis, R.S., Peterson, B.A., Shanks, T., 1983, MNRAS, 205, 605.
 Beers T. C., Flynn K., Gebhardt K., 1990, AJ, 100, 32.
 Borgani S., et al., 1997, New Astron., 1, 321.
 Colless M., et al. (2dFGRS Team), 2001, MNRAS, 328, 1039.
 Collins C.A., et al., 2000, MNRAS, 319, 939.
 Couchman H. M. P., Thomas P. A., Pearce F. R., 1995, ApJ, 452, 797.
 Croft R.A.C., Dalton G.B., Efstathiou G., Sutherland W.J., Maddox S.J., 1997, MNRAS, 291, 305.
 Davis M., Peebles P.J.E., 1983, ApJ, 267, 465.
 Domínguez M.J., Zandivarez A., Martínez H.J., Merchán M.E., Muriel H., Lambas D.G., 2002, MNRAS, 335, 825.
 Eisenstein, D., & Hu, W., 1998, ApJ, 496, 605.
 Feldman H.A., Kaiser N., Peacock J.A., 1994, ApJ, 426, 23.
 Girardi M., Biviano A., Giuricin G., Mardirossian F. & Mezzetti M., 1993, ApJ, 404, 38.
 Girardi M., Giuricin G., 2000, ApJ, 540, 45.
 Girardi M., Boschini W., da Costa L.N., 2000, A&A, 353, 57.
 Governato F., Babul A., Quinn T., Tozzi P., Baugh C. M., Katz N., Lake, G., 1999, MNRAS, 307, 949.
 Hoyle F., Baugh C.M., Shanks T., Ratcliffe A., 1999, MNRAS, 309, 659.
 Huchra J.P., Geller M.J., 1982, ApJ, 257, 423.
 Jing Y., Zhang J., 1988, A&A, 190, L21.
 Kaiser N., 1987, MNRAS, 227, 1.
 Lahav O., et al. (2dFGRS Team), 2002, MNRAS, 333, 961.
 Landy S.D., Szalay A.S., 1993, ApJ, 412, 64.
 Maia M.A.G., da Costa L.N., 1990, ApJ, 349, 477.
 Martínez H.J., Zandivarez A., Domínguez M.J., Merchán M.E., Lambas D.G., 2002a, MNRAS, 333, L31.
 Martínez H.J., Zandivarez A., Merchán M.E., Domínguez M.J., 2002b, MNRAS, 337, 1441.
 Merchán M.E., Maia M.A.G., Lambas D.G., 2000, ApJ, 545, 26.
 Merchán M.E., Zandivarez A., 2002, MNRAS, 335, 216.
 Netterfield, C. B. et al., 2002, ApJ, 571, 604.
 Norberg P., et al. (2dFGRS Team), 2002, MNRAS, 336, 907.
 Padilla N.D., Baugh C.M., 2002, MNRAS, 329, 431.
 Padilla N.D., Merchán M.E., Valotto C.A., Lambas D.G., 2001, ApJ, 554, 873.
 Padilla N.D., Lambas D.G., 2003a, accepted for publication in MNRAS, astro-ph/0302308.
 Padilla N.D., Lambas D.G., 2003b, accepted for publication in MNRAS, astro-ph/0302310.
 Percival W.J., et al. (2dFGRS Team), 2001, MNRAS, 327, 1297.
 Press W.H., Flannery B.P., Teukolsky S.S. & Vetterling W.T., Numerical Recipes, Cambridge University Press, 1986
 Ramella M., Geller M.J., Huchra J.P., 1990, ApJ, 353, 51.
 Ratcliffe, A., Shanks, T., Parker, Q.A., & Fong, R. 1998, MNRAS, 296, 191.
 Sheth R.K., Tormen G., 1999, MNRAS, 308, 119.
 Sheth R.K., Mo H.J., Tormen G., 2001, MNRAS, 323, 1.
 Spergel et al. (WMAP Team), 2003, astro-ph/0302209.
 Trasarti-Battistoni R., Invernizzi G., Bonometto S.A., 1997, ApJ, 475, 1.
 Verde L., et al. (2dFGRS Team), 2002, MNRAS, 335, 432.
 Zandivarez A., Domínguez M.J., Ragone C.J., Muriel H., Martínez H.J., 2002, MNRAS, in press.